

Generalized Rashba spin-orbit coupling for cold atoms

Gediminas Juzeliūnas,¹ Julius Ruseckas,² and Jean Dalibard³

¹*Institute of Theoretical Physics and Astronomy,
Vilnius University, A. Goštauto 12, Vilnius LT-01108, Lithuania*

²*Institute of Theoretical Physics and Astronomy,
Vilnius University, A. Goštauto 12, Vilnius F-01108, Lithuania*

³*Laboratoire Kastler Brossel, CNRS, UPMC, Ecole Normale Supérieure, 24 rue Lhomond, 75005 Paris, France*

(Dated: May 26, 2018)

We study the possibility for generating a new type of spin-orbit coupling for the center-of-mass motion of cold atoms, using laser beams that resonantly couple N atomic internal ground states to an extra state. After a general analysis of the scheme, we concentrate on the tetrapod setup ($N = 4$) where the atomic state can be described by a three-component spinor, evolving under the action of a Rashba-Dresselhaus-type spin-orbit coupling for a spin 1 particle. We illustrate a consequence of this coupling by studying the negative refraction of atoms at a potential step, and show that the amplitude of the refracted beam is significantly increased in comparison to the known case of spin 1/2 Rashba-Dresselhaus coupling. Finally we explore a possible implementation of this tetrapod setup, using stimulated Raman couplings between Zeeman sublevels of the ground state of alkali-metal atoms.

PACS numbers: 37.10.Vz, 37.10.Jk

I. INTRODUCTION

The electron's spin degree of freedom plays a key role in the emerging area of semiconductor spintronics [1–3]. A first scheme for a semiconductor device is the spin field-effect Datta-Das transistor (DDT). It was proposed 20 years ago [4] and implemented recently [5]. Atomic and polaritonic analogs of the electron spin transistor have also been suggested [6, 7]. An important ingredient of the DDT is the spin-orbit coupling of the Rashba [8–10] or Dresselhaus [11, 12] types. This Rashba-Dresselhaus (RD) coupling scheme is described by a vector potential which can be made proportional to the spin-1/2 operator of a particle within a plane [13]. It applies to electrons [3, 9, 10] or atoms with two relevant internal states [14–22].

In the case of atoms, the spin-orbit coupling can be generated using two counterpropagating light beams [17–19, 22] (or two standing waves [16, 20, 21]) and a third beam propagating in an orthogonal direction, the beams being coupled to the atoms in a tripod scheme [15, 23, 24]. The tripod atoms have two degenerate internal dressed states known as *dark states*, which are immune to atom-light coupling. The center-of-mass motion of the dark-state atoms is described by a two-component spinor and is equivalent to the motion of a spin-1/2 particle with spin-orbit coupling [16–22] of the RD type.

In the present article we investigate the possibility to generalize the RD spin-orbit coupling scheme to spins larger than 1/2. We show that this can be achieved using cold atoms with more than two internal dark states. We start our analysis with the general scheme in which N laser beams couple N atomic internal ground states to a common excited state, thus forming the N -pod setup shown in Fig. 1. In the $(N+1)$ -dimensional Hilbert space, we identify $N - 1$ dark states, that is, zero-energy eigen-

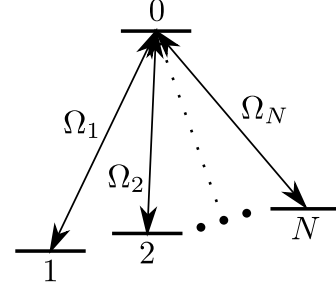


FIG. 1: N -pod configuration. An atomic state $|0\rangle$ is coupled to N different atomic states $|j\rangle$, $j = 1, \dots, N$ by N resonant laser fields.

states of the atom-light Hamiltonian that are superpositions of the N ground states and are immune to atom-light coupling.

Subsequently, we analyze the tetrapod case ($N = 4$) for which the center-of-mass motion of the dark-state atoms is described by a three-component spinor and thus corresponds to the motion of a spin-1 particle. We show that the resulting spin-orbit coupling can be made of the RD type and yields three cylindrically symmetric dispersion branches. Two of them are similar to those for the familiar RD spin-1/2 Hamiltonian, so the atom can exhibit the well-known quasirelativistic behavior [18, 20] for small wave vectors. Furthermore there is an extra branch with a flat dispersion around zero momentum. The formation of the latter branch leads to interesting phenomena, such as a possibility to have a negative refraction at a potential step, characterized by a larger amplitude as compared to the spin-1/2 case.

Finally we explore a possible implementation of the tetrapod scheme for alkali-metal atoms using Raman transitions. To avoid a strong heating due to spontaneous emission, all the states forming the tetrapod

scheme are chosen among the Zeeman sublevels of the atomic ground state, and are coupled by far-detuned Raman lasers beams.

II. THE N -POD SCHEME

A. Atomic Hamiltonian

We are interested in the center-of-mass motion of atoms in the field of several light beams. The atoms are characterized by N internal ground states $|1\rangle, |2\rangle, \dots, |N\rangle$, which are resonantly coupled to an extra state $|0\rangle$ by laser beams. This provides the N -pod configuration shown in Fig. 1. Note that the state $|0\rangle$ does not necessarily represent an electronic excited level; it can be a sublevel of the atomic ground state coupled to the states $|1\rangle, |2\rangle, \dots, |N\rangle$ via stimulated Raman transitions. A more detailed discussion on practical implementation is presented in the Sec. VIII.

The Hamiltonian describing the motion of an atom in the presence of the light beams is

$$H_0 = \frac{\mathbf{p}^2}{2m} + V_0 + V_1 \quad (1)$$

where m is the atomic mass and $\mathbf{p} = -i\hbar\nabla$ the atomic momentum operator. The terms V_0 and V_1 describe the atom-light interaction in the N -pod configuration and a possible additional external potential, respectively. We assume for simplicity that all couplings $|j\rangle \leftrightarrow |0\rangle$, $j = 1, \dots, N$ are resonant, so that V_0 reads using the interaction representation and the rotating wave approximation:

$$V_0 = \hbar \sum_{j=1}^N \Omega_j(\mathbf{r}) |0\rangle\langle j| + \text{H.c.}, \quad (2)$$

where Ω_j is the Rabi frequency that couples the internal state $|j\rangle$ to the common state $|0\rangle$, with $j = 1, 2, \dots, N$. The coupling V_0 can be rewritten as

$$V_0 = \hbar\Omega(\mathbf{r}) \left[|0\rangle\langle B(\mathbf{r})| + |B(\mathbf{r})\rangle\langle 0| \right], \quad (3)$$

with

$$|B\rangle = \frac{1}{\Omega} \sum_{j=1}^N \Omega_j^* |j\rangle, \quad \Omega^2 = \sum_{j=1}^N |\Omega_j|^2. \quad (4)$$

Here $|B\rangle$ is the so-called bright (coupled) state and Ω is the total Rabi frequency.

The diagonalization of the atom-light interaction potential V_0 is straightforward:

(a) The coupling between the bright state $|B\rangle$ and the state $|0\rangle$ with a strength equal to the Rabi frequency Ω in Eq. (3) gives rise to the two eigenstates

$$|\pm\rangle = (|B\rangle \pm |0\rangle) / \sqrt{2}, \quad (5)$$

with energies $\pm\hbar\Omega$.

(b) The remaining orthogonal $(N - 1)$ -dimensional subspace corresponds to dark states. We denote $|D_n\rangle$, $n = 1, \dots, N - 1$ an orthonormal basis of this subspace. All dark states are eigenstates of the Hamiltonian \hat{H}_0 with zero eigenenergy: $\hat{H}_0|D_n\rangle = 0$. They are orthogonal to the bright state and to the state $|0\rangle$: $\langle B|D_n\rangle = \langle 0|D_n\rangle = 0$.

Although the eigenenergies of the dark states are position-independent, the states $|D_n\rangle$ depend on the atomic position through the spatial variation of the Rabi frequencies Ω_j . This leads to the appearance of the gauge potentials to be considered next.

B. Adiabatic motion of dark-state atoms

We now suppose that the atoms are prepared in the dark-state subspace, and that they move sufficiently slowly to remain in this manifold. This adiabatic approximation is justified if the light fields are strong enough, so that the energy difference $\pm\hbar\Omega$ between the dark-state manifold and the other eigenstates $|\pm\rangle$ of V_0 is large compared to the detuning due to Doppler shifts. The atomic state-vector $|\Phi\rangle$ can then be expanded on the dark-state basis

$$|\Phi\rangle = \sum_{j=1}^{N-1} \Psi_j(\mathbf{r}) |D_j(\mathbf{r})\rangle, \quad (6)$$

where $\Psi_j(\mathbf{r})$ is the wave function for the center-of-mass motion of the atom in the j th dark state. The atomic center-of-mass motion is described by an $(N - 1)$ -component wave function

$$\Psi = \begin{pmatrix} \Psi_1 \\ \dots \\ \Psi_{N-1} \end{pmatrix} \quad (7)$$

obeying the Schrödinger equation

$$i\hbar \frac{\partial}{\partial t} \Psi = H\Psi, \quad (8)$$

with the Hamiltonian

$$H = \frac{1}{2m} (-i\hbar\nabla - \mathbf{A})^2 + \Phi + V. \quad (9)$$

The potentials governing the atomic center-of-mass motion \mathbf{A} , Φ , and V are $(N - 1) \times (N - 1)$ matrices. Here \mathbf{A} and Φ are the geometric potentials that emerge due to the spatial dependence of the atomic dark states [15, 25–29]. The matrix $\mathbf{A}(\mathbf{r})$ represents a non-Abelian vector potential, with the matrix elements

$$\mathbf{A}_{n,m} = i\hbar \langle D_n(\mathbf{r}) | \nabla D_m(\mathbf{r}) \rangle, \quad n, m = 1, \dots, N - 1. \quad (10)$$

The matrix $\Phi(\mathbf{r})$ is an effective scalar potential known as the Born-Huang potential. It can be expressed through

the matrix elements of the vector potential between the dark states and the bright state $|B\rangle \equiv |D_0\rangle$:

$$\Phi_{n,m} = \frac{1}{2m} \mathbf{A}_{n,0} \cdot \mathbf{A}_{0,m}, \quad n, m = 1, \dots, N-1. \quad (11)$$

The matrix $V(\mathbf{r})$ represents the restriction of $V_1(\mathbf{r})$ to the dark state subspace. For simplicity we assume in the following that (i) the matrix elements of V_1 between the dark-state manifold and the states $|B\rangle$ or $|0\rangle$ are negligible, so that V_1 cannot cause any significant departure of atoms from the dark-state manifold; (ii) V is proportional to the identity matrix in the dark state subspace, so that it does not break the gauge symmetry of (\mathbf{A}, Φ) . For the particular case of alkali-metal atoms, this occurs when the trapping is provided by far-detuned laser beams. The confinement potential is then the same for all sublevels of the electronic ground state, in particular for the states $|j\rangle$ ($j = 1, \dots, N$) considered here.

The non-Abelian vector potential \mathbf{A} provides a curvature (or effective “magnetic” field)

$$\mathbf{B} = \nabla \times \mathbf{A} + \frac{1}{i\hbar} \mathbf{A} \times \mathbf{A}. \quad (12)$$

The first term represents the usual curl. Note that the second term $\mathbf{A} \times \mathbf{A}$ does not vanish in general, since the Cartesian components of the vector potential \mathbf{A} do not necessarily commute (i.e. the vector potential is non-Abelian). Therefore in contrast to the Abelian case, even a constant vector potential can produce a nonzero curvature and thus provide nontrivial topological effects, leading, for example, to unusual dispersion curves.

III. EFFECTIVE FIELDS GENERATED BY PLANE-WAVE LASER BEAMS

A. Dark states and gauge potentials

From now on we focus on the case where the laser beams represent plane running waves characterized by wave vectors \mathbf{k}_j , $j = 1, \dots, N$. We suppose that the N Rabi frequencies have equal amplitudes and read

$$\Omega_j = \frac{1}{\sqrt{N}} \Omega e^{i\mathbf{k}_j \cdot \mathbf{r}}, \quad j = 1, 2, \dots, N. \quad (13)$$

At this stage the directions of the wave vectors \mathbf{k}_j are still arbitrary; we will address some specific geometries in Secs. V and VI.

A convenient orthogonal set of $N-1$ normalized dark states is

$$|D_n\rangle = \frac{1}{\sqrt{N}} \sum_{j=1}^N |j\rangle e^{i2\pi j n/N - i\mathbf{k}_j \cdot \mathbf{r}}, \quad (14)$$

with $n = 1, 2, \dots, N-1$. Note that the bright state given by Eqs. (4) and (13) has the form of Eq. (14) with $n = 0$, so we will use in the following the notation $|D_0\rangle \equiv |B\rangle$.

Equations (10) and (14) provide the matrix elements of the vector potential

$$\mathbf{A}_{n,m} = \frac{\hbar}{N} \sum_{j=1}^N \mathbf{k}_j e^{i2\pi j(m-n)/N}. \quad (15)$$

It is evident that the vector potential $\mathbf{A}_{n,m}$ depends only on the difference $n-m$, i.e. $\mathbf{A}_{n,m} = \mathbf{A}_{n-m,0}$.

Since the vector potential given by Eq. (15) is constant in space, the effective magnetic field (12) simplifies to $i\hbar\mathbf{B} = \mathbf{A} \times \mathbf{A}$. Using Eq. (15), it can be expressed in terms of the off-diagonal matrix elements of the vector potential $\mathbf{A}_{n,0}$ and $\mathbf{A}_{0,m}$:

$$\mathbf{B}_{n,m} = \frac{i}{\hbar} \mathbf{A}_{n,0} \times \mathbf{A}_{0,m}. \quad (16)$$

B. Vector potential and angular momentum

We now address the following question: Can the vector potential \mathbf{A} be made proportional to a three-dimensional (3D) angular momentum operator \mathbf{J} , that is, $\mathbf{A} = \gamma\mathbf{J}$, where γ is a constant? If the answer was positive, this would allow one to achieve a three-dimensional RD-type coupling. This would be formally similar to the effective spin-orbit interaction discussed in [30], arising from non-Abelian gauge fields in molecular physics. However as we see now, one cannot use the present scheme to achieve $\mathbf{A} \propto \mathbf{J}$.

The angular momentum operator is known to obey the following relations:

$$\mathbf{J} \times \mathbf{J} = i\hbar\mathbf{J}. \quad (17)$$

If $\mathbf{A} = \gamma\mathbf{J}$, the cross product of the vector potential should be proportional to the vector potential itself: $\gamma\mathbf{A} \times \mathbf{A} = i\hbar\mathbf{A}$ or simply $\gamma\mathbf{B} = \mathbf{A}$. Using Eq. (16), the last relationship would lead to

$$\gamma\mathbf{A}_{n,0} \times \mathbf{A}_{n,0}^* = -i\hbar\mathbf{A}_{n-m,0}, \quad n, m = 1, \dots, N-1. \quad (18)$$

Multiplying Eq. (18) by $\mathbf{A}_{m,0}^*$, the left-hand side of the resultant equation is zero. Thus one arrives at

$$\mathbf{A}_{m,0}^* \cdot \mathbf{A}_{n-m,0} = 0. \quad (19)$$

Equation (19) should hold for all possible values of n and m . In particular, by taking $m = 1$ and $n = 2$, one finds $\mathbf{A}_{1,0}^* \cdot \mathbf{A}_{1,0} = 0$. This equation can be fulfilled only if $\mathbf{A}_{1,0} = 0$. Then by taking $m = 1$, the relationship (18) yields that $\mathbf{A}_{n-1,0} = \mathbf{A}_{n+p,p+1} = 0$ for integer n and p . This means that the vector potential $\mathbf{A} = \gamma\mathbf{J}$ should be identically equal to zero.

In this way, we have proved that when using the N -pod scheme with plane waves of equal amplitudes it is not possible to generate a nonzero vector potential which is proportional to the 3D angular momentum operator \mathbf{J} . In other words, it is not possible to produce a 3D spin-orbit coupling of the RD type using the N -pod scheme.

Yet one can get a two-dimensional (2D) RD coupling by means of the N -pod scheme. This includes not only the usual spin-1/2 RD coupling but also a generalized 2D RD coupling for the spin-1 case, as we shall see later on.

IV. PLANE MATTER-WAVE SOLUTIONS

We suppose in the following that the external potential V is uniform in space. In this case the Schrödinger equation (8) has plane-wave solutions:

$$\Phi_{\mathbf{k}}(\mathbf{r}, t) = \Psi_{\mathbf{k}} e^{i\mathbf{k}\cdot\mathbf{r} - \omega_{\mathbf{k}} t}, \quad (20)$$

where $\omega_{\mathbf{k}}$ is an eigenfrequency and $\Psi_{\mathbf{k}}$ is a \mathbf{k} -dependent spinor:

$$\Psi_{\mathbf{k}} = \begin{pmatrix} \Psi_{1,\mathbf{k}} \\ \dots \\ \Psi_{(N-1),\mathbf{k}} \end{pmatrix}. \quad (21)$$

Note that the direction of the wave vector \mathbf{k} is arbitrary and it is not related to the wave vectors of the light beams \mathbf{k}_j .

The \mathbf{k} -dependent spinor $\Psi_{\mathbf{k}}$ obeys the stationary Schrödinger equation

$$H_{\mathbf{k}} \Psi_{\mathbf{k}} = \hbar \omega_{\mathbf{k}} \Psi_{\mathbf{k}},$$

with the \mathbf{k} -dependent Hamiltonian

$$H_{\mathbf{k}} = \frac{\hbar^2}{2m} k^2 - \frac{\hbar}{m} \mathbf{A} \cdot \mathbf{k} + \frac{1}{2m} \mathbf{A}^2 + \Phi + V. \quad (22)$$

Exploiting Eqs. (11) and (15), the scalar term $\mathbf{A}^2/2m + \Phi$ takes the form

$$\left(\frac{1}{2m} \mathbf{A}^2 + \Phi \right)_{n,m} = \frac{\hbar^2}{2m} \frac{1}{N} \sum_{j=1}^N \mathbf{k}_j^2 e^{i \frac{2\pi}{N} (m-n)j}. \quad (23)$$

If the wave vectors of all the Rabi frequencies have the same modulus $\mathbf{k}_j^2 = 2\kappa^2$, the term

$$\frac{1}{2m} \mathbf{A}^2 + \Phi = \frac{\hbar^2 \kappa^2}{m} \hat{I} \quad (24)$$

is proportional to the unit matrix \hat{I} for any arrangement of the wave vectors (both planar and 3D). In this case the Hamiltonian (22) simplifies to

$$H_{\mathbf{k}} = \frac{\hbar}{2m} \left(\hbar k^2 - 2\mathbf{A} \cdot \mathbf{k} + 2\hbar \kappa^2 \right) + V. \quad (25)$$

If the external trapping potential V is proportional to the unit matrix, the eigenvectors $\Psi_{\mathbf{k}}^{\beta}$ of the Hamiltonian $H_{\mathbf{k}}$ are also the eigenvectors of the operator $A_{\mathbf{k}} = \mathbf{A} \cdot \mathbf{k}/k$ representing the projection of the vector potential along the wave vector,

$$A_{\mathbf{k}} \Psi_{\mathbf{k}}^{\beta} = -\hbar \kappa \beta \Psi_{\mathbf{k}}^{\beta}, \quad (26)$$

where the dimensionless parameter $\beta \equiv \beta_{\mathbf{k}}$ depends generally on the wave-vector \mathbf{k} . The corresponding eigenvalues of the Hamiltonian $H_{\mathbf{k}}$ are

$$\hbar \omega_{\mathbf{k}}^{\beta} = \frac{\hbar^2}{2m} \left[(k + \beta \kappa)^2 + (2 - \beta^2) \kappa^2 \right] + V. \quad (27)$$

For $\mathbf{k} = \mathbf{0}$ all the eigenenergies $\hbar \omega_{\mathbf{k}}^{\beta}$ are equal and do not depend on the branch parameter β . Consequently all dispersion branches merge to $\omega_0^{\beta} \equiv \omega_0$ at the origin where $k = 0$. To find the eigenstates and the eigenenergies for $k \neq 0$, one needs to specify the arrangement of the wave vectors \mathbf{k}_j .

V. PLANAR GEOMETRY

A. Wave vectors on a regular polygon

Let us analyze a situation where the wave vectors \mathbf{k}_j are situated in a plane and form a regular polygon

$$\mathbf{k}_j = \sqrt{2}\kappa [-\cos \alpha_j \mathbf{e}_x + \sin \alpha_j \mathbf{e}_y] \quad (28)$$

$$= -\kappa \left(e^{i\alpha_j} \mathbf{e}_+ + e^{-i\alpha_j} \mathbf{e}_- \right), \quad (29)$$

with $\mathbf{e}_{\pm} = \frac{1}{\sqrt{2}}(\mathbf{e}_x \pm i\mathbf{e}_y)$, where $\alpha_j = 2\pi j/N$ is the angle between the wave vector and the x axis. The scalar and vector potentials, Eqs. (11) and (15), take the form

$$\Phi_{n,m} = \frac{\hbar^2 \kappa^2}{2m} (\delta_{m,1} \delta_{n,1} + \delta_{m,N-1} \delta_{n,N-1}), \quad (30)$$

$$\mathbf{A}_{n,m} = -\hbar \kappa \sum_{\pm} \mathbf{e}_{\pm} \delta_{n,m \pm 1}. \quad (31)$$

The vector potential is thus a tridiagonal matrix whose elements are proportional to $\mathbf{e}_x \pm i\mathbf{e}_y$, whereas the scalar potential $\Phi_{n,m}$ is a diagonal matrix with nonzero elements only for $n = m = 1$ or $n = m = N - 1$.

Note that the matrices A_x and A_y , are proportional to the x and y components of the angular momentum operator \mathbf{J} only for the tripod ($N = 3$) and tetrapod ($N = 4$) schemes. In these cases the scalar potential is proportional to J_z^2 .

The projection of $\mathbf{A}_{n,m}$ along the wave vector is

$$(A_{\mathbf{k}})_{n,m} = -\frac{\hbar \kappa}{\sqrt{2}} \left(\delta_{n,m+1} e^{i\varphi} + \delta_{n,m-1} e^{-i\varphi} \right), \quad (32)$$

where φ is the angle between the wave vector \mathbf{k} and the x axis. The eigenvectors of this operator are

$$\Psi_{\mathbf{k}}^{\beta} = \sqrt{\frac{2}{N}} \begin{pmatrix} \sin\left(\frac{\pi q}{N}\right) \\ \sin\left(2\frac{\pi q}{N}\right) e^{i\varphi} \\ \dots \\ \sin\left((N-1)\frac{\pi q}{N}\right) e^{i(N-2)\varphi} \end{pmatrix}, \quad (33)$$

with $q = 1, \dots, N-1$. The corresponding eigenvalues are given by Eq. (26) with

$$\beta = \sqrt{2} \cos\left(\frac{\pi q}{N}\right). \quad (34)$$

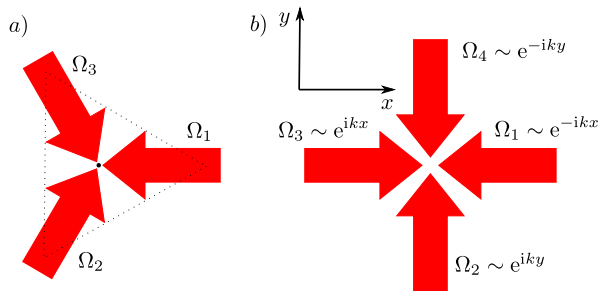


FIG. 2: (Color online) Planar arrangement of laser beams for tripod (a) and tetrapod (b) setups.

It is to be emphasized that the dimensionless parameter β does not depend on \mathbf{k} for this particular geometry. The vectors $\Psi_{\mathbf{k}}^{\beta}$ represent eigenstates of the Hamiltonian with eigenenergies ω_k^{β} given by Eqs. (27) and (34). This provides $N - 1$ dispersion branches.

B. Tripod setup

Consider first the tripod setup ($N = 3$) in which the wave vectors \mathbf{k}_j form an equilateral triangle [Fig. 2(a)]. The parameter β featured in Eqs. (26) and (34) then takes the values $\hbar\beta/\sqrt{2} = \pm\hbar/2$, representing the eigenvalues of the projection of a spin-1/2 on a given axis. In such a situation the operator \mathbf{A} is related to the spin 1/2 operator $\hbar\boldsymbol{\sigma}_{\perp}$, providing the RD coupling along the xy plane as in the previous studies [16–22]:

$$\mathbf{A} = -\hbar\kappa\boldsymbol{\sigma}_{\perp}/\sqrt{2}. \quad (35)$$

It is noteworthy that the present setup produces a cylindrically symmetric spin-orbit coupling in a more straightforward manner than the previously suggested tripod schemes. Those schemes involved two counterpropagating light beams [17–19, 22] (or two standing waves [16, 20, 21]) and a third beam propagating in an orthogonal direction. Consequently, one needed to add a detuning potential and make the amplitudes of the Rabi frequencies asymmetric in order to have dispersion curves of the RD-type, with the proper cylindrical symmetry [16–22]. On the contrary, for the present regular polygon arrangement of wave vectors, the dispersion relation is naturally symmetric as long as the amplitudes of all four Rabi frequencies are equal.

C. Tetrapod setup

For $N = 4$ one arrives at the tetrapod setup involving two pairs of counterpropagating laser fields shown in Fig. 2(b). In this case the vector potential reads

$$\mathbf{A} = \frac{\hbar\kappa}{\sqrt{2}} \begin{pmatrix} 0 & -\mathbf{e}_x + i\mathbf{e}_y & 0 \\ -\mathbf{e}_x - i\mathbf{e}_y & 0 & -\mathbf{e}_x + i\mathbf{e}_y \\ 0 & -\mathbf{e}_x - i\mathbf{e}_y & 0 \end{pmatrix}. \quad (36)$$

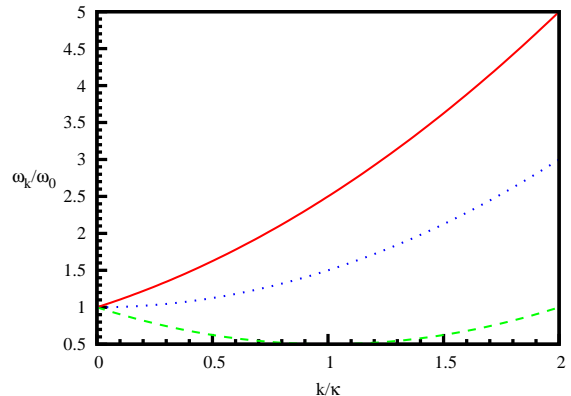


FIG. 3: (Color online) Dispersion curves for the tetrapod scheme calculated using Eq. (40) for $V = 0$. Here $\omega_0 = \hbar\kappa^2/m$.

The possible values for the parameter β featured in Eq. (26) are $\hbar\beta = 0, \pm\hbar$, representing the eigenvalues of the component of a spin 1 along a given axis. Consequently the operator \mathbf{A} is proportional to the projection \mathbf{J}_{\perp} of a spin 1 operator along the xy plane

$$\mathbf{A} = -\kappa\mathbf{J}_{\perp}, \quad \mathbf{J}_{\perp} = J_x\mathbf{e}_x + J_y\mathbf{e}_y. \quad (37)$$

The scalar potential can be represented in terms of the z component of the spin operator

$$\Phi = \frac{\hbar^2\kappa^2}{2m}J_z^2. \quad (38)$$

The eigenstates and the eigenenergies of the Hamiltonian are now

$$\Psi_{\mathbf{k}}^{\pm 1} = \frac{1}{2} \begin{pmatrix} 1 \\ \pm\sqrt{2}e^{i\alpha} \\ e^{2i\alpha} \end{pmatrix}, \quad \Psi_{\mathbf{k}}^0 = \frac{1}{\sqrt{2}} \begin{pmatrix} -1 \\ 0 \\ e^{2i\alpha} \end{pmatrix}, \quad (39)$$

and

$$\hbar\omega_k^{\beta} = \frac{\hbar^2}{2m} \left(k^2 + 2\kappa k\beta + 2\kappa^2 \right) + V, \quad \beta = 0, \pm 1. \quad (40)$$

For $\beta = \pm 1$ the dispersion curves shown in Fig. 3 are analogous to those of the spin-1/2 RD model. An additional dispersion curve with $\beta = 0$ represents a parabola centered at $k = 0$.

The dispersion curve with $\beta = -1$ has its minimum at $\hbar\omega = \hbar^2\kappa^2/2m$, whereas the other two dispersion branches have minima at the double energy $\hbar\omega = \hbar^2\kappa^2/m$ (for $V = 0$). Therefore, all dispersion curves have a strictly positive minimum energy. This nonzero minimum originates from the micromotion of the atom in the light field, caused by nonadiabatic transitions between the dark and bright states [31, 32]. The associated kinetic energy gives rise to the scalar potential given by Eq. (30), which has a nonzero contribution even when acting on the dark states.

Finally, we note an important difference in the ‘‘topology’’ of the eigenfunctions for the RD spin-1/2 and spin-1 problems, even though the $\beta = \pm 1$ branches have the same dispersion in the two cases: The wave functions $\Psi_{\mathbf{k}}^{\beta}$ exhibit a π Berry’s phase in k space in the spin-1/2 case, whereas this Berry’s phase is absent for the spin-1.

VI. TETRAHEDRON GEOMETRY

In this section we present an example of a nonplanar setup, which has some advantages with respect to the planar configuration investigated in the previous section, because it leads to a simpler scalar potential. We consider again the tetrapod setup ($N = 4$) with wave vectors \mathbf{k}_j arranged in a regular tetrahedron geometry:

$$\hat{\mathbf{k}}_j \cdot \hat{\mathbf{k}}_{j'} = -\frac{1}{3}, \quad j \neq j'. \quad (41)$$

where $\hat{\mathbf{k}}_j = \mathbf{k}_j/k_j$ is a unit vector. More precisely, we choose

$$\mathbf{k}_{1,3} = \kappa'(\pm \mathbf{e}_y \sqrt{2} - \mathbf{e}_z), \quad \mathbf{k}_{2,4} = \kappa'(\pm \mathbf{e}_x \sqrt{2} + \mathbf{e}_z). \quad (42)$$

Using Eq. (15), the vector potential then reads

$$\mathbf{A} = \frac{\hbar \kappa'}{\sqrt{2}} \begin{pmatrix} 0 & -\mathbf{e}_x + i\mathbf{e}_y & \sqrt{2}\mathbf{e}_z \\ -\mathbf{e}_x - i\mathbf{e}_y & 0 & -\mathbf{e}_x + i\mathbf{e}_y \\ \sqrt{2}\mathbf{e}_z & -\mathbf{e}_x - i\mathbf{e}_y & 0 \end{pmatrix}. \quad (43)$$

For atoms moving in the xy plane the vector potential can be expressed in terms of a spin-1 operator in the xy plane: $\mathbf{A}_{\perp} = -\kappa' \mathbf{J}_{\perp}$. Hence we obtain as before a RD-type spin-orbit coupling for the atomic motion in the xy plane, characterized by the dispersion relation shown in Fig. 3. Yet we are now dealing with a 3D problem, so the same dispersion also characterizes the atomic motion along two other planes perpendicular to the vectors $\mathbf{e}_x + \mathbf{e}_y$ and $\mathbf{e}_x - \mathbf{e}_y$. By making an atomic lattice along these directions, the atomic tunneling will be influenced by a spin-1 RD coupling, thus extending the previous studies of spin-1/2 RD coupling in lattices [33]. This will be investigated in a separate study.

A distinguished feature of the tetrahedron geometry is that the scalar potential is proportional to the unit matrix \hat{I} :

$$\Phi = \frac{\hbar^2 \kappa'^2}{2m} \hat{I}. \quad (44)$$

Thus for atoms placed in a 3D lattice, there is no energy mismatch between different dark states located in adjacent sites. This contrasts with the planar tetrapod case (Eq. (38)), where the spin components are likely to get frozen in the lattice because tunneling matrix elements are normally much smaller than the atomic recoil energy, which gives the scale for the scalar potential.

It is noteworthy that the z component of the vector potential given by Eq. (43) is not proportional to J_z .

Hence, one cannot generate a 3D Hamiltonian with RD-type spin-orbit coupling for all directions of the atomic motion. This is a particular case of the general conclusion reached in the Sec. III B.

VII. TRANSMISSION BY A POTENTIAL STEP

A spectacular consequence of spin-orbit RD coupling is the negative refraction and reflection that occurs when a matter wave is incident on a potential step. The problem was investigated for spin-1/2 atoms [18, 34] and electrons [35]. In this case one can calculate relatively easily the transmission and reflection of the atomic wave packet. For small wave vectors of the incident atoms, $k \ll \kappa$, the transmission probability is close to unity at zero angle of incidence. Here the parameter κ characterizes the strength of the spin-orbit interaction, see Eq. (35). This nearly complete transmission is a manifestation of the Klein paradox appearing also for electron tunneling in graphene [36]. For a nonzero angle of incidence, the transmission probability is less than 1 and decreases with increasing angle. Furthermore the transmitted matter wave experiences negative refraction [18], similar to the case of electrons in graphene [37].

Particles with a spin larger than 1/2 have additional degrees of freedom, which modifies the continuity conditions at the potential step. This can lead to a significant increase of the transmission probability of atoms, as we show now for particles submitted to a spin-1 RD coupling.

A. The Hamiltonian

We consider in this section the motion of a particle in the xy plane described by the Hamiltonian

$$H = \frac{1}{2m} (\hat{\mathbf{p}}^2 + 2\hbar\kappa\hat{\mathbf{p}} \cdot \mathbf{J}_{\perp} + 2\hbar^2\kappa^2) + V(x) \quad (45)$$

where $\mathbf{J}_{\perp} = J_x \mathbf{e}_x + J_y \mathbf{e}_y$ is the projection of spin-1 operator onto the xy plane. Such a Hamiltonian can be obtained using the tetrapod setups described in the Secs. V C and VI. The external potential $V(x)$ is given by the step function along x

$$V(x) = \begin{cases} 0, & x \leq 0 \\ V_0, & x > 0 \end{cases} \quad (46)$$

with $V_0 > 0$. It is convenient to introduce the wave vector $k_0 = 2mV_0/\hbar^2\kappa$ characterizing the height of the barrier.

For a constant potential the eigenvalue equation has plane-wave solutions (20) characterized by the spinor part $\Psi_{\mathbf{k}}^{\beta}$ [Eq. (39)]. The corresponding eigenvalues $\hbar\omega_{\mathbf{k}}^{\beta}$ are given by Eq. (40) with $k = \sqrt{k_x^2 + k_y^2}$ and are plotted in Fig. 3. Additionally there can be evanescent wave solutions localized in the vicinity of the potential step in

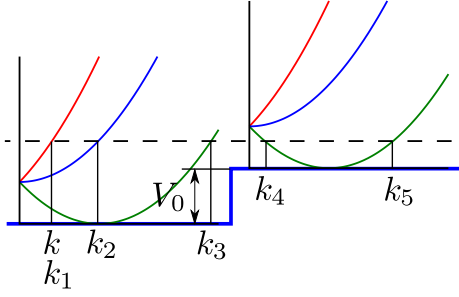


FIG. 4: (Color online) Wave numbers of reflected and transmitted waves and energy conservation at the potential step.

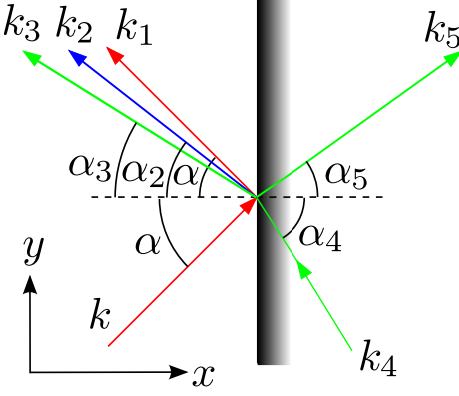


FIG. 5: (Color online) Reflection and transmission of atoms at a potential step. In addition there is an evanescent transmitted wave with $\mathbf{k}_6 = k_y \mathbf{e}_y + iq \mathbf{e}_x$.

the $x > 0$ region. In that case we have $k_x = iq$ with $q > 0$, giving

$$k = \sqrt{k_y^2 - q^2}, \quad q^2 < k_y^2. \quad (47)$$

For the present problem, only the evanescent wave with $\beta = 0$ will play a role,

$$\Psi_{k_y, q}^0 = c_{k_y, q}^0 \begin{pmatrix} -1 \\ 0 \\ \frac{q+k_y}{q-k_y} \end{pmatrix}, \quad (48)$$

where $c_{k_y, q}^\beta$ is the normalization factor.

B. Incident waves with $\beta = 1$

In this paragraph we restrict our analysis to the case where the incident atom is prepared in the upper dispersion branch ($\beta = 1$) in the region $x < 0$. Denoting its wave vector by \mathbf{k} , the incident wave is

$$\Psi_{\text{in}} = \Psi_{\mathbf{k}}^1 e^{i\mathbf{k} \cdot \mathbf{r}}. \quad (49)$$

The potential step is assumed to be high enough,

$$k_0 > k^2/\kappa + 2k, \quad (50)$$

so that there can be no propagating transmitted waves with chirality $\beta = 0$ or $\beta = 1$ (see Fig. 4). At the same time, to allow for propagation of plane waves in the region $x > 0$ for the lower dispersion branch $\beta = -1$, the step height should not be too large:

$$k_0 < \kappa + k^2/\kappa + 2k. \quad (51)$$

The directions of reflected and transmitted waves are depicted in Fig. 5. The reflected waves generally contain all three components,

$$\Psi_{\text{ref}} = r_1 \Psi_{\mathbf{k}_1}^1 e^{i\mathbf{k}_1 \cdot \mathbf{r}} + r_2 \Psi_{\mathbf{k}_2}^0 e^{i\mathbf{k}_2 \cdot \mathbf{r}} + r_3 \Psi_{\mathbf{k}_3}^{-1} e^{i\mathbf{k}_3 \cdot \mathbf{r}}, \quad (52)$$

where $k_1 = k$, $k_2 = \sqrt{k^2 + 2\kappa k}$ and $k_3 = k + 2\kappa$. The reflection angles are $\pi - \alpha$, $\pi - \alpha_2$, and $\pi - \alpha_3$, with $\alpha_2 = \arcsin[\sin(\alpha)k/k_2]$ and $\alpha_3 = \arcsin[\sin(\alpha)k/k_3]$. The transmitted waves are

$$\Psi_{\text{tr}} = t_4 \Psi_{\mathbf{k}_4}^{-1} e^{i\mathbf{k}_4 \cdot \mathbf{r}} + t_5 \Psi_{\mathbf{k}_5}^{-1} e^{i\mathbf{k}_5 \cdot \mathbf{r}} + t_6 \Psi_{\mathbf{k}_6}^0 e^{i\mathbf{k}_6 \cdot \mathbf{r}}, \quad (53)$$

where $k_4 = \kappa - \sqrt{(k+\kappa)^2 - k_0\kappa}$, $k_5 = \kappa + \sqrt{(k+\kappa)^2 - k_0\kappa}$, and $k_6 = k^2 + 2\kappa k - k_0\kappa$ (see Fig. 4). The first and second transmitted waves experience negative and positive refraction, respectively, and propagate at the angles $\pi - \alpha_4$ and α_5 , where $\alpha_4 = \arcsin[\sin(\alpha)k/k_4]$ and $\alpha_5 = \arcsin[\sin(\alpha)k/k_5]$. On the other hand, due to the condition (50) the third transmitted wave with the helicity $\beta = 0$ is an evanescent one along the x axis and thus is characterized by the wave vector $\mathbf{k}_6 = k_y \mathbf{e}_y + iq \mathbf{e}_x$, with $k_y = k \sin \alpha$ and $q = \sqrt{k_y^2 - k^2}$. Note that there is no evanescent transmitted wave in the upper dispersion branch ($\beta = 1$) because it cannot comply with the momentum conservation along the interface in addition to the energy conservation.

The multicomponent wave function and its first derivative in the x direction are required to be continuous at the barrier ($x = 0$), providing six equations containing six unknown coefficients r_1 , r_2 , r_3 , t_4 , t_5 , and t_6 . Of special interest is the situation where $k_0 = 4k$. In this case the wave number of the first refracted wave coincides with the wave number of the incident wave, $k_4 = k$, so the angle of refraction is equal to the angle of incidence for the first reflected wave. $\alpha_4 = \alpha$.

The analytical solution for the six coefficients is generally complicated. It is instructive to obtain approximate solutions for small wave vectors and small angles of incidence, $k \ll \kappa$ and $\alpha \ll 1$. In such a case one can restrict to reflected (52) and transmitted (53) waves containing only the contributions of \mathbf{k}_1 , \mathbf{k}_2 , \mathbf{k}_4 , and \mathbf{k}_6 . The transmitted wave with \mathbf{k}_6 represents a rapidly decaying evanescent wave characterized by a spinor component given by Eq. (48) with $q \gg k_y$:

$$\Psi_{\mathbf{k}_6}^0 \approx \frac{1}{\sqrt{2}} \begin{pmatrix} -1 \\ 0 \\ 1 \end{pmatrix}. \quad (54)$$

The continuity of the wave function at $x = 0$ gives

$$\Psi_{\mathbf{k}}^1 + r_1 \Psi_{\mathbf{k}_1}^1 + r_2 \Psi_{\mathbf{k}_2}^0 e^{i\mathbf{k}_2 \cdot \mathbf{r}} = t_4 \Psi_{\mathbf{k}_4}^{-1} + t_6 \Psi_{\mathbf{k}_6}^0. \quad (55)$$

In addition, we require continuity of the derivative in the x direction for the component with $\beta = 0$, which is the largest:

$$k_2 \cos(\pi - \alpha_2) r_2 \Psi_{\mathbf{k}_2}^0 = i q a \Psi_{\mathbf{k}_6}^0 \quad (56)$$

Here $k_4 \approx k_0/2 - k$ and $\alpha_2 \approx \sqrt{k/2\kappa} \sin(\alpha)$, with $k_2 = \sqrt{2\kappa k}$ and $q \approx \sqrt{\kappa(k_0 - 2k)}$. Using the spinors (39) and (54) one obtains the following solution to Eqs. (55) and (56):

$$t_4 = \frac{2 \cos \alpha}{\cos \alpha + \cos \alpha_4} e^{i(\alpha + \alpha_4)} \quad (57)$$

$$r_1 = \frac{\cos \alpha_4 - \cos \alpha}{\cos \alpha + \cos \alpha_4} e^{i2\alpha} \quad (58)$$

$$r_2 = \frac{\sqrt{k_0 - 2k}}{\sqrt{k + i\sqrt{k_0/2 - k}}} \cos \alpha \tan\left(\frac{\alpha + \alpha_4}{2}\right) e^{i\alpha} \quad (59)$$

The calculated reflection and transmission coefficients r_1 and t_4 obey the probability conservation up to terms of the order of $O(\alpha^2)$:

$$|r_1|^2 + \frac{\cos \alpha_4}{\cos \alpha} |t_4|^2 \approx 1. \quad (60)$$

If the barrier height is such that $k_0 = 4k$, we have $\alpha_4 = \alpha$. In that case $|t_4| \approx 1$ and $|r_1| \approx 0$ leading to an almost perfect negative refraction, at the exact opposite refraction angle, provided $k \ll \kappa$ and the angles of incidence are not too large.

Figure 6 presents the comparison of the transmission probabilities for the spin-1 and spin-1/2 RD coupling using the exact numerical solutions of the continuity equations at the boundary $x = 0$. For the spin-1/2 case the incident wave is also prepared in the upper dispersion branch. The figure shows a marked increase in the transmission probability for small angles of incidence in the case of spin 1. Note that the transmitted waves experience negative refraction both for the spin-1 and the spin-1/2 cases.

VIII. IMPLEMENTATION OF THE TETRAPOD SETUP WITH ALKALI-METAL ATOMS

We now discuss a possible implementation of the tetrapod scheme. We consider the case of alkali-metal atoms, which are the most frequently used in current experiments. In order to avoid a strong heating due to spontaneous emission, we study the case where the state $|0\rangle$ is actually one of the Zeeman sublevels of the ground state. The states $|j\rangle$ (with $j = 1, \dots, 4$) are also Zeeman sublevels of the ground state, and the coupling between the state $|0\rangle$ and a state $|j\rangle$ is provided by a pair of laser beams that induce a Raman transition under the condition of the two-photon resonance. The use of Raman transitions in this context is an extension to the tetrapod case of a recent proposal [38] to implement a Λ -type

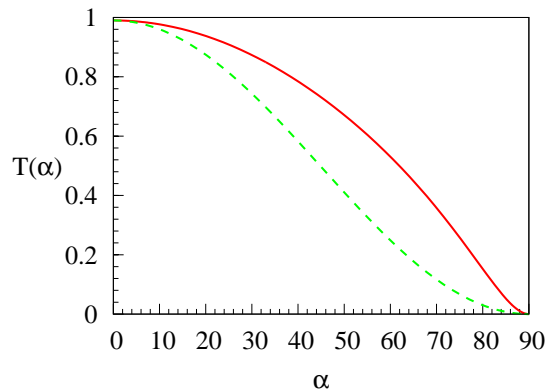


FIG. 6: (Color online) Transmission probability of negatively refracted atoms at a potential step as a function of the angle of incidence α for a spin-1 (solid red) and spin-1/2 (dashed green) systems. The parameters used for the calculation are $k/\kappa = 0.1$ and $k_0/\kappa = 0.4$ for both systems.

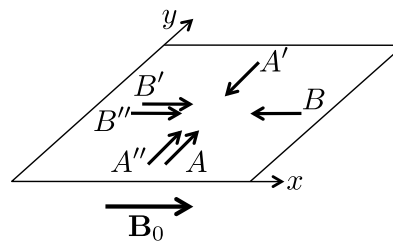


FIG. 7: Directions of the laser beams used for implementing the tetrapod coupling scheme with alkali-metal atoms, via stimulated Raman transitions.

scheme for the generation of an effective magnetic field by means of the counterpropagating laser beams [32, 39].

We recall that the electronic ground level $nS_{1/2}$ of alkali-metal atoms is split by hyperfine interaction in two sublevels with angular momenta $F = I + 1/2$ and $F = I - 1/2$, where I is the nuclear spin. We consider in the following the case $I = 3/2$ that is relevant for lithium (${}^7\text{Li}$, $n = 2$), sodium (${}^{23}\text{Na}$, $n = 3$) or rubidium (${}^{87}\text{Rb}$, $n = 5$). In order to minimize the rate of spontaneous emission processes, we restrict to Raman transitions that are far detuned from the resonance with the “true” excited states $nP_{1/2}$ or $nP_{3/2}$ of the D_1 or D_2 transitions. More precisely the typical one-photon detuning of the beams involved in the Raman process is chosen much larger than the hyperfine structure of the excited level $nP_{1/2}$ or $nP_{3/2}$ (0.8 GHz for the hyperfine splitting of the level $5P_{1/2}$ of ${}^{87}\text{Rb}$). At the same time the one-photon detuning should be smaller than the fine structure splitting, that is, the difference between the energies of $nP_{1/2}$ and $nP_{3/2}$ (7000 GHz for ${}^{87}\text{Rb}$). When the one-photon detuning exceeds the hyperfine splitting, the nucleus angular momentum does not play any role in the selection rules that determine the allowed transitions for photon absorption or emission. For the D_1 (D_2) transition, the allowed couplings are the same as between a

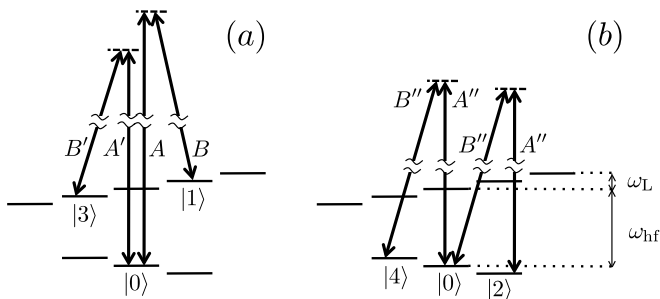


FIG. 8: Implementation of the tetrapod scheme for alkali-metal atoms with two hyperfine levels of angular momentum $F = 1$ and $F = 2$. The laser couplings involved in this scheme correspond to stimulated Raman transitions between hyperfine states of the ground atomic level. We choose $|0\rangle \equiv |F = 1, m_F = 0\rangle$. (a) The laser beams A , A' , B and B' induce the transitions $|0\rangle \rightarrow |1\rangle \equiv |F = 2, m_F = 1\rangle$ and $|0\rangle \rightarrow |3\rangle \equiv |F = 2, m_F = -1\rangle$. (b) The laser beams A'' and B'' induce the transitions $|0\rangle \rightarrow |2\rangle \equiv |F = 1, m_F = 1\rangle$ and $|0\rangle \rightarrow |4\rangle \equiv |F = 1, m_F = -1\rangle$.

spin-1/2 ground level and a spin-1/2 (3/2) excited level. In particular, the only allowed Raman transitions correspond to a change $\Delta m_J = 0$ or $\Delta m_J = \pm 1$ of the azimuthal quantum number m_J .

A scheme that fulfills the aforementioned constraints is represented in Figs. 7 and 8. The atomic motion along the z direction is supposed to be frozen thanks to a trapping potential $m\omega_z^2 z^2/2$ such that $\hbar\omega_z$ is much larger than the atomic kinetic energy. The atom is placed in a uniform magnetic field B_0 directed along the x direction. The role of this magnetic field is to allow for a selective Raman excitation between two given Zeeman sublevels. More precisely the Larmor frequency $\omega_L = \mu_B B_0/\hbar$ (μ_B is the Bohr magneton) is chosen much larger than the two-photon (Raman) Rabi frequency Ω . Typically we choose $\omega_L/2\pi$ on the order of a few MHz (i.e. B_0 on the order of a few Gauss) and $\Omega/2\pi$ in the range $10^5 - 10^6$ Hz. The latter choice is sufficient to ensure that the splitting $\hbar\Omega$ between the dark-state manifold and the states $|\pm\rangle$ is large compared to the two-photon Doppler shift, as required for the adiabatic approximation to be valid. The state $|0\rangle$ is chosen equal to the $|F = 1, m_F = 0\rangle$ sublevel and the states $|j\rangle$ with $j = 1, \dots, 4$ are the $|F = 2, m_F = \pm 1\rangle$ and $|F = 1, m_F = \pm 1\rangle$ sublevels. Here the quantization axis is the x axis, parallel to the direction of the magnetic field \mathbf{B}_0 . As indicated in Fig. 8(a), the transition between $|0\rangle$ and $|1\rangle \equiv |F = 2, m_F = +1\rangle$ is driven by a pair of laser beams (A, B) with a frequency difference equal to $\omega_{\text{hf}} + \omega_L/2$, where ω_{hf} is the hyperfine splitting between the $F = 1$ and $F = 2$ manifolds ($\omega_{\text{hf}}/2\pi$ is on the order of 7 GHz for ^{87}Rb). The laser beam A propagates along the y axis (wave vector $k\mathbf{e}_y$, where \mathbf{e}_y is a unit vector). It is linearly polarized along x , so that it carries no angular momentum along the x axis. The laser beam B propagates along the x axis (wave vector $-k\mathbf{e}_x$) and is circularly (σ_-) polarized. In the tran-

sition $|0\rangle \rightarrow |1\rangle$ the momentum change of the atom is $\hbar\mathbf{k}_1 = \hbar k(\mathbf{e}_x + \mathbf{e}_y)$. One can readily check that the transition $|0\rangle \rightarrow |1\rangle$ is the only one that is driven resonantly by this pair of beams, thanks to the fact that the Landé factors are opposite for the $F = 1$ and $F = 2$ manifolds, as one can see in Fig. 8(a). Similarly, the transition between $|0\rangle$ and $|3\rangle \equiv |F = 2, m_F = -1\rangle$ is driven by a pair of laser beams (A', B') with a frequency difference equal to $\omega_{\text{hf}} - \omega_L/2$. The beam A' propagates along y with wave vector $-k\mathbf{e}_y$ and is linearly polarized along x . The beam B' propagates along x with wave vector $k\mathbf{e}_x$ and is circularly (σ_+) polarized. The atomic momentum change in the transition $|0\rangle \rightarrow |3\rangle$ is $\hbar\mathbf{k}_3 = -\hbar\mathbf{k}_1$. The difference in the frequencies of A and A' is chosen large enough so that no transition is driven with a significant probability by the pairs of beams (A, B') and (A', B).

The two remaining states of the tetrapod configuration are $|2\rangle \equiv |F = 1, m_F = +1\rangle$ and $|4\rangle \equiv |F = 1, m_F = -1\rangle$. The coupling between these states and the state $|0\rangle$ is provided by a single pair of laser beams (A'', B''), as in the recent experiment [38], in which the Λ (ladder) type coupling was generated within the Zeeman sublevels of the $F = 1$ manifold. The wave vector of A'' is $k\mathbf{e}_y$ and this beam is linearly polarized along x . The beam B'' propagates along x with wave vector $k\mathbf{e}_x$ and is circularly (σ_+) polarized. The frequency difference between the beam A'' and B'' is $\omega_L/2$ so that the pair (A'', B'') resonantly drives the transition $|0\rangle \rightarrow |2\rangle$ with a momentum transfer $\hbar\mathbf{k}_2 = \hbar k(\mathbf{e}_x - \mathbf{e}_y)$, and the transition $|0\rangle \rightarrow |4\rangle$ with a momentum transfer $\hbar\mathbf{k}_4 = -\hbar\mathbf{k}_2$. Note that here again we take advantage of the different signs of the Landé factors of the $F = 1$ and $F = 2$ manifolds: The pair of beams (A'', B'') cannot resonantly drive a transition between two sublevels of the $F = 2$ manifold [see Fig. 8(b)]. Note also that another consequence of two-photon processes is a modification of the energies of the states $|j\rangle$, via the absorption and stimulated emission of photons in the same laser beam. It can be accounted for by including these energy shifts in the choice of the two-photon detunings and, for example, by taking advantage of the (small) second-order Zeeman shift.

This configuration therefore constitutes a suitable implementation of the scheme discussed in the first part of this article. The momentum transfers $\hbar\mathbf{k}_j = \hbar k(\pm\mathbf{e}_x \pm \mathbf{e}_y)$ form a square in the xy plane shown in Fig. 2(b) (subject to the rotation of the coordinate system by 45°). The intensities of the various beams can be adjusted so that all Rabi frequencies Ω_j are equal, once the Clebsch-Gordan coefficients associated to each Raman transition have been taken into account (note that the two-photon Rabi frequencies for $|0\rangle \rightarrow |2\rangle$ and $|0\rangle \rightarrow |4\rangle$ transitions are equal by construction). With a one-photon detuning of 3 nm, which represents 1/5 of the fine structure splitting for rubidium atoms, the residual photon scattering rate is below 1 s^{-1} for a two-photon Rabi frequency $\Omega/(2\pi) = 10^5$ Hz. The corresponding heating rate is thus small enough to provide enough time for the investigation of the RD coupling studied in this article.

IX. CONCLUSIONS

In this article we have explained how to produce a spin-orbit coupling of the RD type for a spin larger than $1/2$. Our scheme makes use of cold atoms with three or more internal dark states so that their quasi-spin is equal to or greater than unity. We have analyzed a general scheme in which N laser beams couple N atomic internal ground states to an extra state, thus forming an N -pod setup of light-matter interaction. In this case the atoms have $N - 1$ dark states representing superpositions of the N ground states that are immune to the atom-light coupling.

We have analyzed in detail the particular case of the tetrapod setup ($N = 4$), in which the center of mass motion of the atoms in their dark state manifold is described by a three-component spinor and thus corresponds to the motion of a spin-1 particle. We have shown that the resulting spin-orbit coupling can be made of the RD type and yields three cylindrically symmetric dispersion branches. Two of them are similar to those known for the familiar RD spin- $1/2$ Hamiltonian, so the atom can exhibit a quasirelativistic behavior [18–20] for small wave vectors. Furthermore, we have shown that there exists an extra branch with a flat dispersion around zero momentum. We have studied the modifications that this extra branch brings to the problem of negative refraction

of matter waves on a potential step, and shown that it enhances the negative refraction probability.

Finally we have discussed a possible implementation of the tetrapod setup with cold alkali-metal atoms. We have shown that in order to avoid heating due to spontaneous emission, it is possible to choose all the states involved in this tetrapod scheme among the various Zeeman sublevels of the ground atomic state. All laser couplings are then provided by stimulated Raman transitions. For rubidium atoms, realistic parameters yield a residual spontaneous emission rate below 1 s^{-1} , which makes the observation of this spin-orbit coupling scheme experimentally feasible.

Acknowledgments

We thank M. Lewenstein and S. Das Sarma for helpful discussions. This work has been supported by the Gilibert program, the Lithuanian Science and Studies Foundation (Grant No. V-34/2009), the Research Council of Lithuania, the Région Ile de France IFRAF, the ANR (Grant No. ANR-08-BLAN-65 BOFL), and the EU projects SCALA and STREP NAMEQUAM. LKB is a mixed research unit No.8552 of CNRS, ENS, and Université Pierre et Marie Curie.

-
- [1] A. Fert, *Rev. Mod. Phys.* **80**, 1517 (2008).
 - [2] P. A. Grünberg, *Rev. Mod. Phys.* **80**, 1531 (2008).
 - [3] I. Zutic, J. Fabian, and S. Das Sarma, *Rev. Mod. Phys.* **76**, 323 (2004).
 - [4] S. Datta and B. Das, *Appl. Phys. Lett.* **56**, 665 (1990).
 - [5] H. C. Koo, J. H. Kwon, J. Eom, J. Chang, S. H. Han, and M. Johnson, *Science* **325**, 1515 (2009).
 - [6] J. Y. Vaishnav, J. Ruseckas, C. W. Clark, and G. Juzeliūnas, *Physical Review Letters* **101**, 265302 (2008).
 - [7] R. Johne, I. A. Shelykh, D. D. Solnyshkov, and G. Malpuech, *arXiv:0911.1621* (2009).
 - [8] E. I. Rashba, *Sov. Phys. Sol. St.* **2**, 1224 (1960).
 - [9] R. Winkler, *Spin-Orbit Coupling Effects in Two-Dimensional Electron and Hole Systems* (Springer, Berlin, 2003).
 - [10] M. Kohda, T. Bergsten, and J. Nitta, *J. Phys. Soc. Jpn.* **77**, 031008 (2008).
 - [11] G. Dresselhaus, *Phys. Rev.* **100**, 580 (1955).
 - [12] J. Schliemann, J. C. Egues, and D. Loss, *Phys. Rev. Lett.* **90**, 146801 (2003).
 - [13] J. Schliemann, D. Loss, and R. M. Westervelt, *Phys. Rev. B* **73**, 085323 (2006).
 - [14] A. M. Dudarev, R. B. Diener, I. Carusotto, and Q. Niu, *Phys. Rev. Lett.* **92**, 153005 (2004).
 - [15] J. Ruseckas, G. Juzeliūnas, P. Öhberg, and M. Fleischhauer, *Phys. Rev. Lett.* **95**, 010404 (2005).
 - [16] T. D. Stanescu, C. Zhang, and V. Galitski, *Phys. Rev. Lett.* **99**, 110403 (2007).
 - [17] A. Jacob, P. Öhberg, G. Juzeliūnas, and L. Santos, *Appl. Phys. B* **89**, 439 (2007).
 - [18] G. Juzeliūnas, J. Ruseckas, M. Lindberg, L. Santos, and P. Öhberg, *Phys. Rev. A* **77**, 011802(R) (2008).
 - [19] M. Merkl, F. E. Zimmer, G. Juzeliūnas, and P. Öhberg, *Europhys. Lett.* **83**, 60001 (2008).
 - [20] J. Y. Vaishnav and C. W. Clark, *Phys. Rev. Lett.* **100**, 153002 (2008).
 - [21] J. Larson and E. Sjöqvist, *Phys. Rev. A* **79**, 043627 (2009).
 - [22] Q. Zhang, J. Gong, and C. Oh, *arXiv:0906.1625* (2009).
 - [23] R. G. Unanyan, M. Fleischhauer, B. W. Shore, and K. Bergmann, *Opt. Commun.* **155**, 144 (1998).
 - [24] R. G. Unanyan, B. W. Shore, and K. Bergmann, *Phys. Rev. A* **59**, 2910 (1999).
 - [25] M. V. Berry, *Proc. R. Soc. A* **392**, 45 (1984).
 - [26] F. Wilczek and A. Zee, *Phys. Rev. Lett.* **52**, 2111 (1984).
 - [27] C. A. Mead, *Rev. Mod. Phys.* **64**, 51 (1992).
 - [28] A. Bohm, A. Mostafazadeh, H. Koizumi, Q. Niu, and J. Zwanziger, *The Geometric Phase in Quantum Systems* (Springer, Berlin, 2003).
 - [29] A. Shapere and F. Wilczek, eds., *Geometric Phases in Physics* (World Scientific, Singapore, 1989).
 - [30] B. Zygelman, *Phys. Rev. Lett.* **64**, 256 (1990).
 - [31] Y. Aharonov and A. Stern, *Phys. Rev. Lett.* **69**, 3593 (1992).
 - [32] M. Cheneau, S. P. Rath, T. Yefsah, K. J. Günter, G. Juzeliūnas, and J. Dalibard, *Europhys. Lett.* **83**, 60001 (2008).
 - [33] N. Goldman, A. Kubasiak, P. Gaspard, and M. Lewen-

- stein, Phys. Rev. A **79**, 023624 (2009).
- [34] G. Juzeliūnas, J. Ruseckas, A. Jacob, L. Santos, and P. Öhberg, Phys. Rev. Lett. **100**, 200405 (2008).
- [35] V. Teodorescu and R. Winkler, Phys. Rev. B **80**, 041311(R) (2009).
- [36] M. I. Katsnelson, K. S. Novoselov, and A. K. Geim, Nat. Phys. **2**, 620 (2006).
- [37] V. V. Cheianov, V. Fal'ko, and B. L. Altshuler, Science **315**, 1252 (2007).
- [38] Y.-J. Lin, R. L. Compton, A. R. Perry, W. D. Phillips, J. V. Porto, and I. B. Spielman, Phys. Rev. Lett. **102**, 130401 (2009).
- [39] G. Juzeliūnas, J. Ruseckas, P. Öhberg, and M. Fleischhauer, Phys. Rev. A **73**, 025602 (2006).